A CVBEM Formulation for Multiple Profiles and Cascades*

Jorge D'Elía† , Mario Storti† , and Sergio Idelsohn† .

Key Words: two-dimensional domain, complex boundary element method, potential flow, numerical methods

AMS 2000 subject classification 26B15 Integration: length, area, volume, 32A55 Singular integrals, 45E99 Integral equations with weakly kernels, 65D30 Numerical integration, 65D32 Quadrature and cubature formulas, 74S15 Boundary element methods

PACS 2008 subject classification 02.30.Rz Integral equations, 02.60.Jh Numerical differentiation and integration, 02.70.Pt Boundary-integral methods, 44.05.+e Analytical and numerical techniques, 47.11.-j Computational methods in fluid dynamics, 47.11.Hj Boundary element methods

Abstract

A numerical algorithm based on the Complex Variable Boundary Element Method (CVBEM) for plane incompressible potential flow around aerofoils and cascades is described. The method is based on the representation of the complex disturbance velocity by means of a Cauchy-type integral around the foil. The Cauchy density function is approximated piecewise linearly and a linear system on the nodal values is obtained by collocation at the nodes. The Kutta condition is imposed via a Lagrange multiplier, in contrast with the least-squares formulation used in a previous work [3]. For cascades, the problem is conformally mapped by a simple hyperbolic function (exponential or hyperbolic tangent) to a related problem with only one profile and one or two poles. Thus, the cascade problem is accurately solved with minor modifications to the single profile code and at the same cost of a single profile computation. Finally, several numerical examples are shown: single Joukowski and NACA profiles, interference coefficients for the flat plate cascade and a plane cascade at the external cylindrical section of an industrial fan.

1 Cauchy representation of the perturbation velocity

Consider a plane flow of an incompressible irrotational fluid around an aerofoil. The potential and stream functions ϕ, ψ are defined such that $(u_x, u_y) = (\partial\phi/\partial x, \partial\phi/\partial y) = (\partial\psi/\partial y, -\partial\psi/\partial x)$, where $\boldsymbol{u} = (u_x, u_y)$ is the velocity vector. As is well known, ϕ and ψ are conjugate harmonic functions and a complex potential $\Phi = \phi + i\psi$ can be defined, which is an analytic function of the complex coordinate $z = x + iy$. The complex velocity is obtained as $W = u_x - iv_x = d\Phi/dz$. Now, the complex velocity is decomposed as an external part coming from the superimposed homogeneous flow $W_\infty = \boldsymbol{u}_\infty e^{-i\alpha}$ (see Fig. 1, left), and a perturbation term $w(z)$ in the form $W(z) = W_\infty + w(z)$. We will see later that for cascade flow W_∞ has to be replaced by the field produced by two poles. Being $W(z)$ analytic in the exterior domain D^-, and continuous in C, it can be shown that the Cauchy integral reduces to:

$$\frac{1}{2\pi i}\int_C \frac{W(t)}{t-z}dt = -W(z) + W_\infty \qquad \text{for } z \in (D^- - C); \tag{1}$$

*This work was supported by the Consejo Nacional de Investigaciones Científicas y Técnicas (CONICET)Universidad Nacional del Litoral (UNL) and Agencia Nacional de Promoción Científica y Tecnológica (ANPCyT), Argentina.

†Centro Internacional de Métodos Computacionales en Ingeniería (CIMEC), Instituto de Desarrollo Tecnológico para la Industria Química (INTEC), UNL-CONICET, Güemes 3450, 3000-Santa Fe, Argentina, ph.: +54-342-451 15 94, fx: +54-342-451 11 69, http://venus.ceride.gov.ar/CIMEC

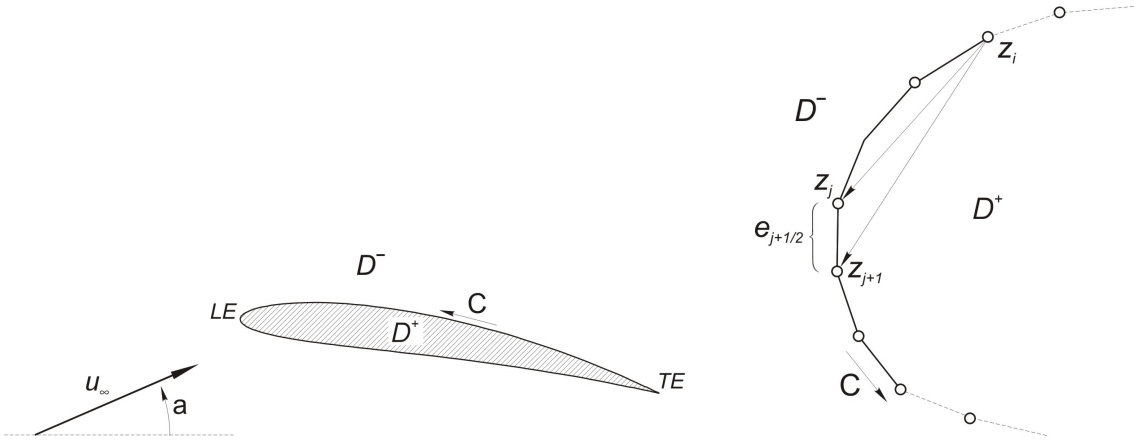

Figure 1: External flow geometry description (left). BEM discretization (right).

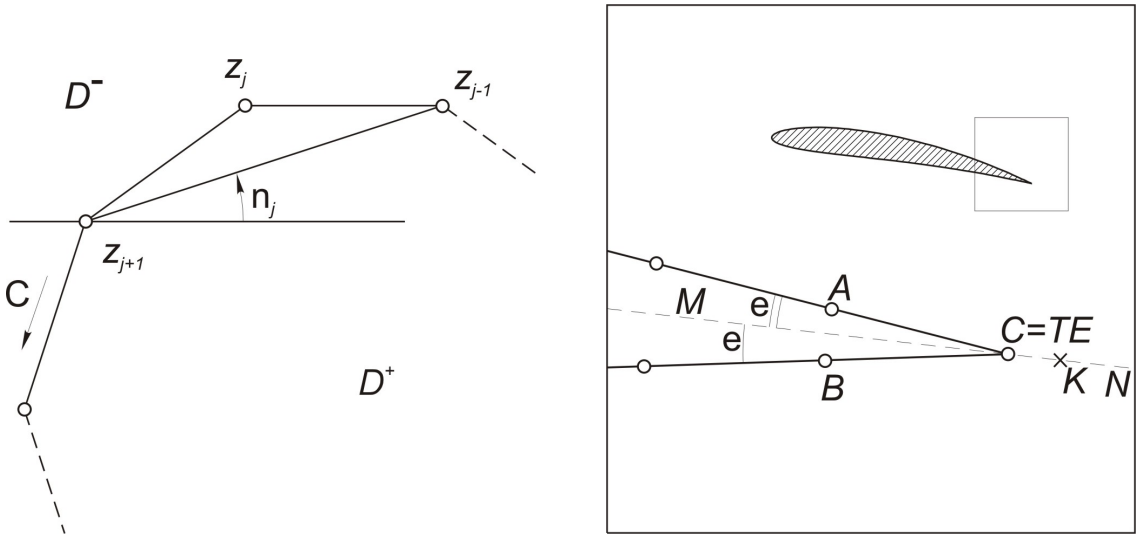

Figure 2: Definition of discrete tangent at node z_j (left). Implementation of Kutta condition (right).

where C is a counterclockwise oriented curve on the aerofoil [3]. For z in C the integral is singular and it must be evaluated in a principal value sense

$$\frac{1}{2\pi i}\int_C \frac{W(t)}{t-z}dt = -\frac{1}{2}W(z) + W_\infty \qquad \text{for } z \in \mathcal{C}. \tag{2}$$

2 Discretization

Our work is based on the paper from Mokry [3]. The contour C is approximated by a closed polygonal joining the nodes $\{z_j\}$, $j = 1, \ldots, N$, numbered in counterclockwise sense. The segments $[z_j, z_{j+1}]$ is called the $e = j + 1/2$-th element (for the first ($e = 1/2$) element, $z_0 = z_N$ is assumed). For the computation of the integral in the left hand side of Eq. (2) we assume that W varies linearly in each element. Thus, the integral can be computed in closed form

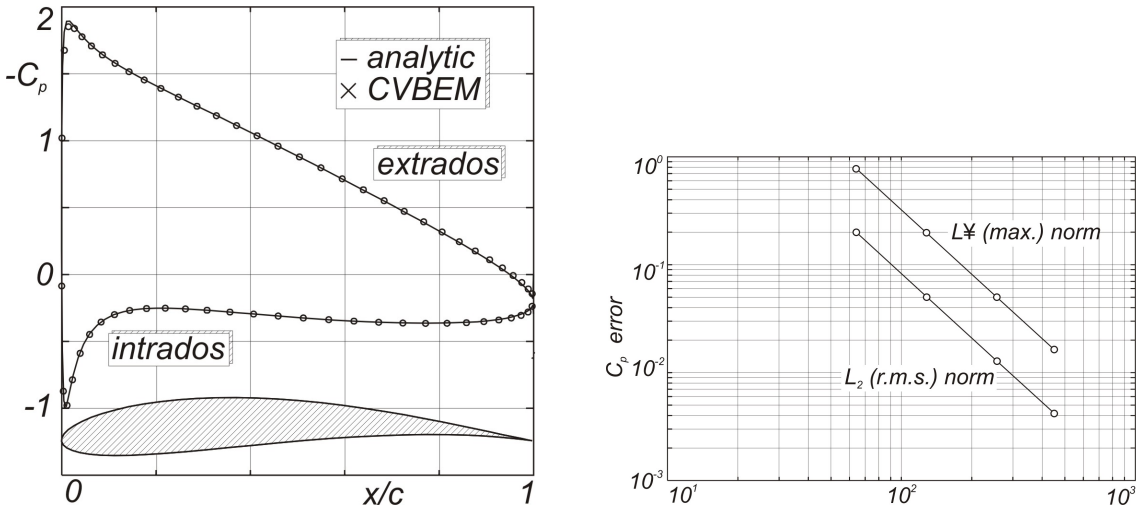

Figure 3: Joukowski profile at $\alpha = 5^{\circ}$, 64 elements (left). Convergence of BEM for an ellipse (right).

as

$$\frac{1}{2}W_i + \frac{1}{2\pi i}W_i \log\left(\frac{z_{i+1}-z_i}{z_{i-1}-z_i}\right) + \frac{1}{2\pi i}\sum_{\substack{e=\frac{1}{2}\\ e\neq i\pm\frac{1}{2}}}^{N-\frac{1}{2}} \left[\left(\frac{z_{e+\frac{1}{2}}-z_i}{z_{e+\frac{1}{2}}-z_{e-\frac{1}{2}}}\right)h_i^e W_{e-\frac{1}{2}} + \left(\frac{z_{e-\frac{1}{2}}-z_i}{z_{e+\frac{1}{2}}-z_{e-\frac{1}{2}}}\right)h_i^e W_{e+\frac{1}{2}}\right] = W_\infty \ ; \tag{3}$$

where $h_i^e = \log[(z_{e+\frac{1}{2}} - z_i)/(z_{e-\frac{1}{2}} - z_i)]$, and $z_{e\pm\frac{1}{2}}$ are the extreme nodes of element e (see Fig. 1, right). Each contribution on the sum, is the corresponding contribution from the integral over the element e. The contributions from the adjacent elements $e = i \pm 1/2$ to node i are singular but their sum is finite and, after a limiting process, the second term of the left hand side is obtained [2]. Replacing Eq. (3) in the integral formulation given by Eq. (2) we arrive to a linear system of N complex equations in the complex nodal velocities $A_{ij}W_j = b_j$, where b_j comes from the homogeneous imposed field W_∞. Now we redefine the nodal velocities to local axes as $W_{\mathrm{loc},j} = W_j e^{i\nu_j}$, where ν_j is the angle between the local tangent at the node (see Fig. 2, left) and the real axis, so that the real and imaginary part of $W_{\mathrm{loc},j}$ are the tangential and normal velocity components. The discrete tangent at node z_j is taken as parallel to the segment joining the adjacent nodes $j \pm 1$. The resulting system is $A_{\mathrm{loc},ij}W_{\mathrm{loc},j} = b_i$.

For the application to external flow problems, the normal velocity at the nodes are zero or a prescribed value, having the signification of a transpiration flux coming from the computation of the boundary layer, for instance. The system has, then, $2N$ real equations with N real unknowns and, to solve this overdetermination, either the real or imaginary part of the system (or a combination of the two) could be taken, but, it can be shown that the conditioning is much better if the real part is taken. The resulting system for the tangential components of the nodal velocities is of the form $K_{ij}v_{\mathrm{tang},j} = b'_i$, $i, j = 1, \ldots, N$, where now all quantities are real. A similar formulation could be based on the complex potential, rather than on complex velocities, but it is somewhat more difficult since, for the lifting case, the former is discontinuous. Moreover, as the quantities of interest are velocities and pressures, with the complex velocity formulation we obtain an $O(N^{-2})$ convergence, in contrast with the $O(N^{-1})$ for the potential-based one.

The treatment given here has a rather *"structured flavor"*, but a non-structured code based on *element-by-element* processing, have been implemented by us.

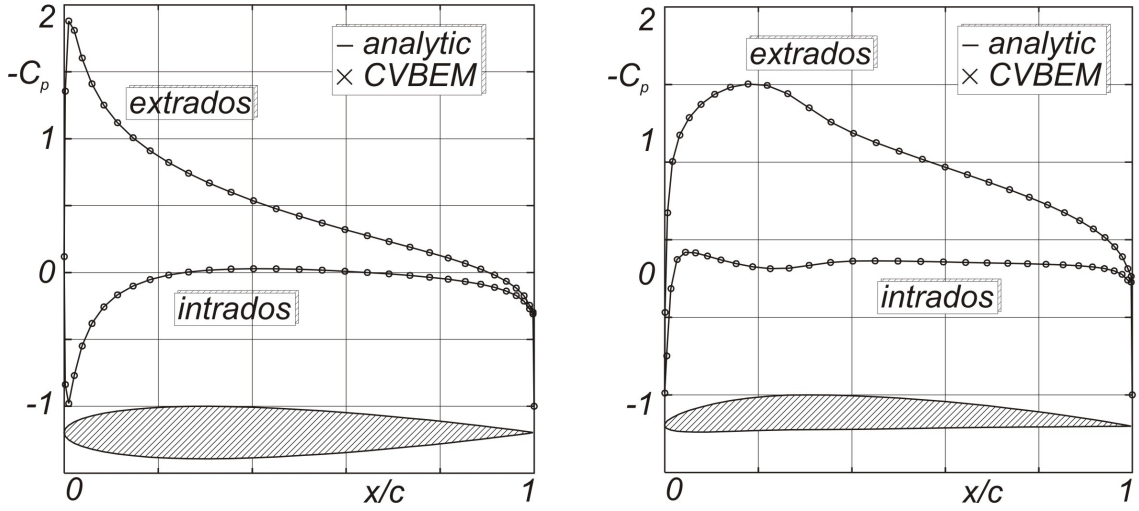

Figure 4: NACA 0012 profile at $\alpha = 5^{\circ}$, 64 elements (left). NACA 4310 profile at $\alpha = 2^{\circ}$, 64 elements (right).

3 The Kutta condition

In the lifting case, one additional condition, namely the Kutta condition, must be added. This is done by imposing null normal component of the velocity to the bisecting line of the trailing edge angle at a neighboring point K of the trailing edge $C = TE$ on the bisecting line (see Fig. 2, right). In practice we have taken $\overline{KC} = \epsilon(\overline{AC} + \overline{BC})$, with $\epsilon = 1/100$. This velocity is computed from the discrete version of Eq. (1) and the resulting discrete linear equation is of the form $c_j v_{\text{tang},j} = d$. As one equation has been added to the system we must either discard one of the original equations, or either add a new unknown. If the matrix $\boldsymbol{K}$ were singular, of rank $N-1$, then any of the original equations could be discarded and replaced by the Kutta condition. However we verified that the matrix is singular only in the limit of infinite nodes. We mean by that, that $N-1$ of the eigenvalues of $\boldsymbol{K}$ are different from 0, i.e. $\lambda_i \geq c > 0$, $i = 1, \ldots, N-1$, and there is an eigenvalue λ_N which approaches 0 as $N \to \infty$. Thus, the result of throwing away a row is not independent of the actual row which is eliminated, and spurious oscillations are found in velocities and pressures near the node whose equation has been thrown away. Another fact, which is observed, is that the matrix $\boldsymbol{K}$ tends to be a symmetric matrix as $N \to \infty$. Then, we impose the Kutta condition via a Lagrange multiplier λ in a symmetric formulation

$$\begin{bmatrix} \boldsymbol{K} & \boldsymbol{c} \\ \boldsymbol{c}^T & 0 \end{bmatrix} \begin{bmatrix} \boldsymbol{v}_t \\ \lambda \end{bmatrix} = \begin{bmatrix} \boldsymbol{b}' \\ d \end{bmatrix} \quad . \tag{4}$$

The overall system is not symmetric since $\boldsymbol{K}$ is not symmetric for finite N. The extension to multiple aerofoils is trivial, and the description will not be given here.

Another possibility, proposed in [3] is to solve the overdetermined system in a least-squares sense. The advantage of the present formulation over the least-squares one is that a much higher condition of the system is obtained with the later.

4 Numerical examples. Application to single aerfoils

4.1 Joukowski profile

In Fig. 3 (left) we see the pressure coefficient computed for a Joukowski profile (12% thickness, 4.6% camber) at an incidence of $\alpha = 5^{\circ}$. The exact distribution is shown as a solid line. The mesh has 64 elements and it has been

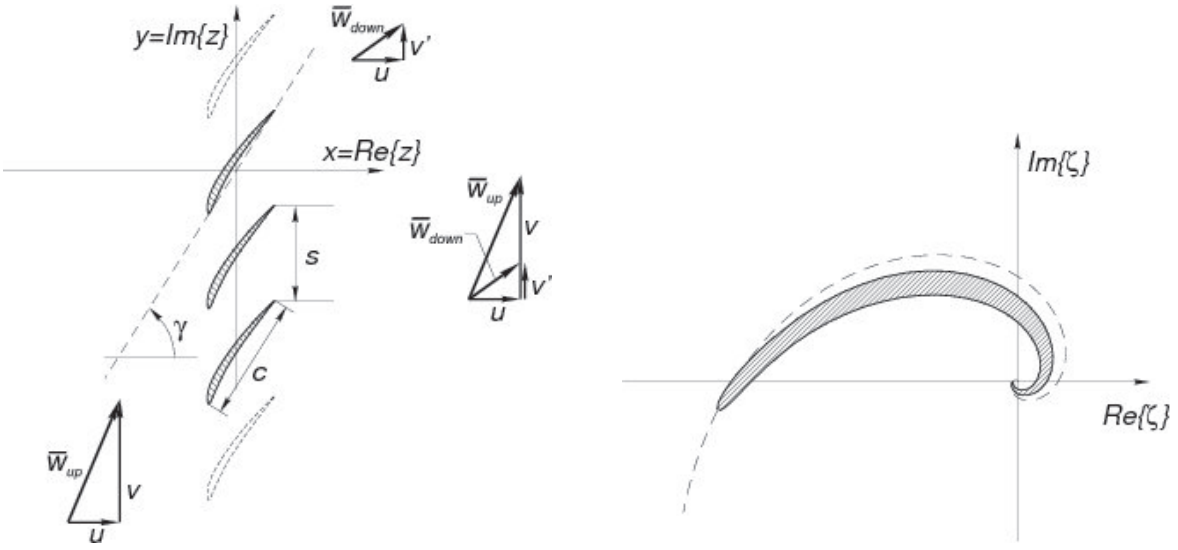

Figure 5: Cascade geometry description (left). Transformed cascade in ζ plane (right).

generated by applying the Joukowski transformation to an homogeneous grid on a circle. In this way, a quadratic distribution of nodes is obtained near the leading and trailing edges. The coincidence is very good, whereas it has been stated [3] that CVBEM is not well suited for profiles having zero angle at the trailing edges.

4.2 Numerical study of convergence

We computed the error for the case of an ellipse $b/a = 0.25$ at incidence $\alpha = 33.75^{\circ}$, for N =64, 128, 256 and 450 nodes. The error in c_p is computed as (r.m.s. error)$^2 = \sum_j [c_{p,j} - (C_{p,\text{ext}})_j]^2$, and (max. error) $= \max_j |c_{p,j} - (C_{p,\text{ext}})_j|$, and they are ploted versus N in a log-log axis (see Fig. 3 (right). The observed convergence rate is $O(N^{-2})$, which is optimal for the approximation used.

4.3 NACA profiles

Regarding profiles with non-zero angle at the trailing edge, we computed the flow around the NACA 0012 at $\alpha = 5^{\circ}$ and NACA 4310 at $\alpha = 2^{\circ}$ with 64 elements profiles and the corresponding c_p distributions at are shown in Fig. 4.

5 Application to plane cascade flow

Consider the geometry shown in Fig. 5 (left). A typical calculation [1] consists in, given the vector velocity upstream W_{up} to compute the vector velocity downstream W_{down} and, also, distributions of pressure and velocity around the aerofoil. By continuity requirements $\Re W_{\text{up}} = \Re W_{\text{down}}$ but, in general, $\Im W_{\text{up}} \neq \Im W_{\text{down}}$, so that we can put $W_{\text{up}} = u - iv$, $W_{\text{down}} = u - iv'$. The deflection of the velocity vector is related to important global quantities, such as compression ratio, net force and power, etc, much in the same way the circulation is in the theory of the single aerofoil. A straightforward application of the method to a cascade of aerofoils is to compute the flow around a finite, but large, number of aerofoils. This procedure has two main drawbacks: firstly, the cost of the computation increases with the cube of the number of aerofoils considered and, secondly, the far field flow deflection can be incorrectly estimated, since a finite deflection at infinity downstream can be generated only by an infinite row of aerofoils [3].
We transform the cascade conformally by $\zeta = \exp(2\pi z/s)$ where s is the spacing of the cascade. The infinity upstream $z_U = -\infty + ib$ is mapped on $\zeta_U = 0$, and the infinity downstream $z_D = +\infty + ib$ is mapped to $\zeta_D = \infty$. It can be

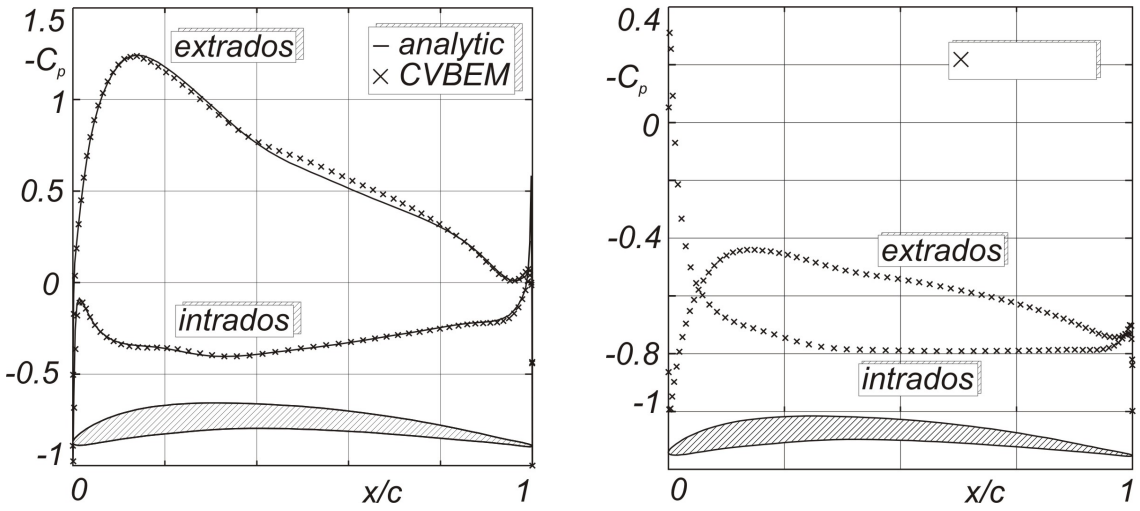

Figure 6: C_p distribution for $s/c = 3.3$ (left). C_p distribution for $s/c = 0.825$ (right).

verified that all the aerofoils in the z-plane are transformed onto the same profile in ζ. Thus, the strategy is to solve the problem in this plane and transforming back the results to the z-plane. As usual, the complex potential is invariant under the transformation, i.e. $\Phi(\zeta) = \Phi(z(\zeta))$. We can, then, obtain the expression for the complex velocity v in the ζ plane near ζ_U as $v = d\Phi/d\zeta = (d\Phi/dz)\,(dz/d\zeta) = W_{\rm up}(s/2\pi\zeta)$. The application of the method is now straightforward since W_∞ is replaced by $W_{\rm ext} = W_{\rm up}s/(2\pi\zeta)$, which modifies only the right hand side of the system of equations. Of course, the geometry is previously transformed on the ζ plane. Once the complex velocities in the ζ plane, v_j are obtained, the corresponding velocities w_j in the z-plane are easily found from

$$w = \frac{d\Phi}{dz} = \frac{d\Phi}{d\zeta} d\zeta/dz = v(2\pi\zeta/s) \ . \tag{5}$$

As only tangential velocities are of interest

$$w_{t,j} = v_{t,j} \left| \frac{2\pi\zeta_j}{s} \right| \ . \tag{6}$$

The circulation around a single aerofoil of the row is computed directly in the ζ plane, since it is invariant under a conformal mapping. The tangential velocity downstream is computed from $\Im W_{\rm up} = \Im W_{\rm down} - \Gamma/s$.
If the downstream velocity is prescribed, the transformation $z = \exp(-2\pi z/s)$ is used, instead. In this way, the infinity downstream is mapped onto $\zeta_D = 0$ and the infinity upstream to $\zeta_U = \infty$, and the remaining computations are similar. If the average velocity is prescribed, which is a rather common situation, then the flow can be computed as in Eq. (5) with two distinct tangential elocities $\Im W_{\rm up_{1,2}}$ and the desired average value can be obtained by superposition. Another, perhaps more elegant, option is to apply the transformation $\zeta = \tanh(\pi z/s)$. Now $\zeta_{U,D} = \pm 1$, and none of the tangential velocities are known, but two linear relations between them and the circulation around the aerofoil can be written, and a linear determined system is obtained again. The treatment described here for cascades is different from that of Mokry.

6 Numerical example. Application to cascade flow

6.1 Tip cylindrical section of an industrial fan

The blade section has a 6% maximum thickness at 22% chord from the leading edge, and 6% maximum camber at 37% chord. Two values of spacing are considered: $s/c = 3.3$ and 0.825. The geometry for the cascade and the blade

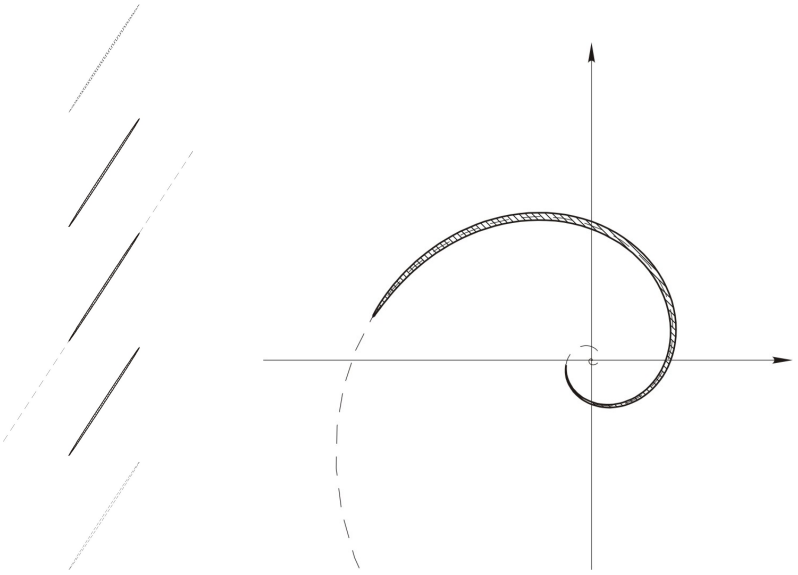

Figure 7: Flat plate cascade at $s/c = 1$ and $\gamma = 70^{\circ}$ (left). Flat plate cascade in ζ plane (right).

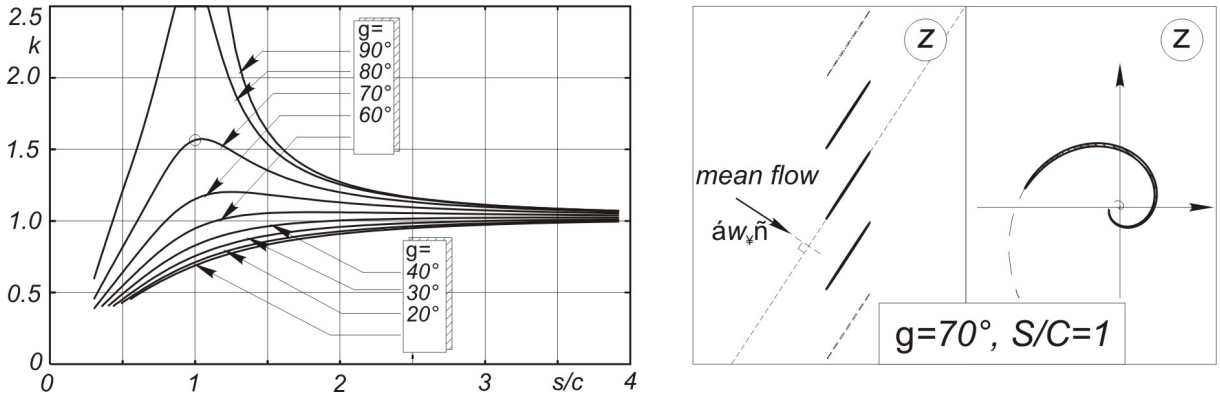

Figure 8: Interference coefficients computed by BEM.

section are shown in Fig. 5 (left) for the case of $s/c = 0.825$. In Fig. 5 (rigth) we see the transformed profile in the ζ plane, and also an undisturbed streamline (a logarithmic helicoid) for flow parallel to the chord. The profile was modelled with 128 elements quadratically refined near the leading and trailing edges. The c_p distribution is shown in Fig. 6 (left and rigth), together with the prediction from another potential model (solid line) based on a Theodorsen transformation This last algorithm is spectrally convergent and we estimate that the given distribution is exact to machine precision.

6.2 Interference coefficients for the flat plate cascade

The interference coefficient [1] is defined as $k_0 = \Gamma(\gamma, s)/\Gamma(\gamma, \infty)$, where $\Gamma(\gamma, s)$ is the circulation around one profile from a cascade of the specified stagger and spacing, for a mean flow $\langle W_\infty \rangle = (W_{\rm up} + W_{\rm down})/2)$ inciding at 90° with the plate (see Fig. 7, left). The value $\Gamma(\gamma, \infty)$ corresponds to the circulation around an isolated plate and for the flat plate at 90° is $\Gamma(\gamma, \infty) = \pi$ (we assume a unitary length for the plate). Fig. 7 (left) corresponds to the actual configuration at $s = 1$, $\gamma = 70^{\circ}$, and Fig. 7 (right) to the transformed foil in the ζ plane. For the computation, the plates have been replaced by very thin ellipses (relative thickness=1%) discretized with 256 elements. The mesh

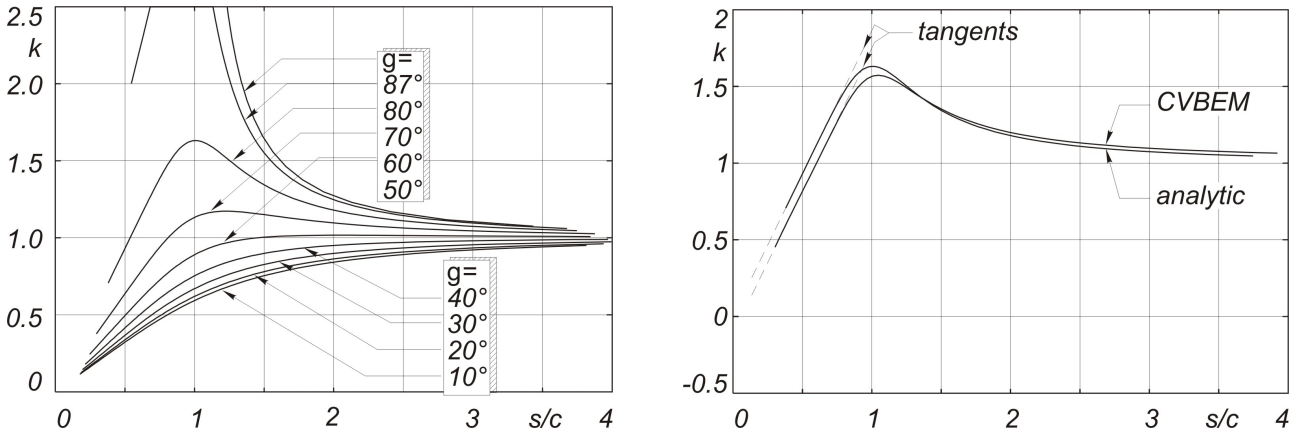

Figure 9: Analytic interference coefficients (left). Finite thickness effect for $\gamma = 70^\circ$ (right).

was constructed applying a Joukowski transformation to a homogeneous grid on a circle. This is a very hard case because of the very small angles at the leading and trailing edges and also because that, at very low spacing, the transformed foil in the ζ plane spirals logarithmically at the origin giving rise to very different element sizes. For instance, at $s/c = 0.3$ and $\gamma = 10^\circ$, the difference in size between the elements at the transformed leading and trailing edges is a factor $\approx 10^8$. The computation have been carried out for $\gamma = 10^\circ, 20^\circ, \ldots, 90^\circ$ and 65 values for s/c interpolated logarithmically between 0.3 and 4. In Figs. 8 and 9 (left) we see the computed coefficients and the exact ones, obtained by conformal mapping. Some small discrepancies are present at low spacing, which we attribute to discretization errors, specially to the finite thickness of the foil actually used. Consider, for instance, the curves for $\gamma = 70^\circ$ which have been superimposed in Fig. 9 (right). The analytic coefficient behaves $\sim s$ for small s, whereas the tangent to the BEM-computed one is parallel but predicts a null k_0 for a small positive s, as it would be expected to occur for a finite thickness foil.

7 Acknowledgement

A. Cardona has participated in fruitful discussions on the formulation of the Kutta condition via a Lagrange multiplier. The authors wish to express their gratitude to *Consejo Nacional de Investigaciones Científicas y Técnicas* (CONICET, Argentina) for its financial support.

References

[1] W. R. Hawthorne, editor. *Aerodynamics of Turbines and Compressors*. Princeton Univ. Press, 1964.

[2] T.V. Hromadka. *The Complex Variable Boundary Element Method*. Springer-Verlag, Berlin, 1984.

[3] M. Mokry. Complex variable boundary element method for external potential flows. In *28th Aerospace Sciences Meeting*, Reno, Nevada, January 8-11 1990.